Electrical Impedance Tomography Reconstruction Using ℓ_1 Norms for Data and Image Terms

Tao Dai and Andy Adler

***Abstract*— Electrical Impedance Tomography (EIT) calculates the internal conductivity distribution within a body from current simulation and voltage measurements on the body surface. Two main technical difficulties of EIT are its low spatial resolution and sensitivity to measurement errors. Image reconstruction using ℓ_1 norms allows addressing both difficulties, in comparison to traditional reconstruction using ℓ_2 norms. A ℓ_1 norm on the data residue term reduces the sensitivity to measurement errors, while the ℓ_1 norm on the image prior reduces edge blurring. This paper proposes and tests a general *lagged diffusivity* type iterative method for EIT reconstructions. ℓ_1 and ℓ_2 minimizations can be flexibly chosen on the data residue and/or image prior parts. Results show the flexibility of the algorithm and the merits of the ℓ_1 solution.**

I. INTRODUCTION

Electrical Impedance Tomography (EIT) images the impedance distribution within a body from electrical stimulation and measurements on the body surface. One of key limitations of EIT is its relatively poor image resolution, which, for 16 electrodes is less than 10% of the body diameter. EIT is a soft field tomography modality, due to the diffusive propagation of electrical current. Thus, the reconstruction of an internal conductivity distribution from boundary data is severely ill-conditioned [1]. In order to calculate a "reasonable" image, regularization techniques are required. Such regularized image reconstructions can be statistically formulated in terms of *a priori* information about image element values and the correlations among them. These correlations are often expressed as generalized Tikhonov regularization; the zeroth order Tikhonov [2], discrete Laplacian filter [3] and weighted diagonal (NOSER) priors [4], [5], etc. Another limitation to the quality of EIT images is measurement errors, which arise from multiple sources, such as RF coupling onto signal wires, electrode malfunction, and subject movement. While it is common to model such measurement noise as Gaussian, such noise sources introduce many more outliers than the the Gaussian model would predict. Most image reconstruction algorithms for EIT search for an image solution, $\hat{\mathbf{x}}$, which minimizes an error expression based on the ℓ_2 norm, *e.g.,*one-step GN method. However, these algorithms are known to blur image regions and be sensitive to data outliers.

It is widely recognized that the Total Variation (TV) (ℓ_1 norm of image spatial gradient) regularization is good at recovering discontinuities in the image while the Least Squares (LS, or ℓ_2 norm) solution is prone to smooth out edges. This is because penalty terms using ℓ_2 norm penalize smooth transitions less than sharp transitions, while ℓ_1 norms penalize only the transition amplitude, and not its slope. Similarly, the ℓ_2 penalty for a data outlier is larger (the difference is squared) than for the ℓ_1. This means the ℓ_1 solution is less perturbed by outliers. However, the ℓ_1 solution involves the minimization of a non-differentiable objective function, and thus cannot be efficiently solved by the traditional optimization methods that minimize a differentiable objective function such as the Steepest Decent and GN method.

In this paper we propose an image reconstruction algorithm based on the lagged-diffusivity method in which the ℓ_1 norm is applied to both the image prior and data fidelity term. This preserves image edges and provides enhanced resistance against data errors. This algorithm has a general iterative structure which enables flexibly choosing different norm strategies, and termination criteria.

II. METHODS

An EIT system with n_E electrodes is considered. Electrodes are applied to a body in a single plane and adjacent current stimulation and voltage measurement are performed. n_E current stimulation patterns are sequentially applied and n_V differential measurements are made for each stimulation. Difference EIT calculates difference data $\mathbf{y} = \mathbf{v}_2 - \mathbf{v}_1$, where $\mathbf{y}, \mathbf{v} \in \mathbb{R}^{n_M}$, $n_M = n_E \times n_V$, and $\mathbf{v}_1$ and $\mathbf{v}_2$ are the vectors or measurements before and after a conductivity change of interest. To improve precision, $\mathbf{v}_1$ is typically averaged over many data frames, at a time when the conductivity distribution may be assumed to be stable; thus. $\mathbf{v}_1$ is assumed noise free.

The model under investigation is a circular finite element model (FEM) which has n_N piecewise elements represented by a vector $\boldsymbol{\sigma} \in \mathbb{R}^{n_N}$. Difference EIT calculates a vector of conductivity change, $\mathbf{x} = \boldsymbol{\sigma}_2 - \boldsymbol{\sigma}_1$ between the present conductivity distribution, $\boldsymbol{\sigma}_2$, and the reference measurement, $\boldsymbol{\sigma}_1$. In this paragraph, $\boldsymbol{\sigma}$ represents conductivity; elsewhere in this paper, σ is the standard deviation. For small variations around $\boldsymbol{\sigma}_1$, the relationship between $\mathbf{x}$ and $\mathbf{y}$ can be linearized as:

$$\mathbf{y} = \mathbf{J}\mathbf{x} + \mathbf{n} \tag{1}$$

where $\mathbf{J} \in \mathbb{R}^{n_M \times n_N}$ is the Jacobian or sensitivity matrix; $\mathbf{n} \in \mathbb{R}^{n_M}$ is the measurement noise which is assumed to

This work was supported by a grant from NSERC Canada

T. Dai is with the Department of System and Computer Engineering, Carleton University, Ottawa, Ontario, Canada. tdai@sce.carleton.ca

A. Adler is with the Department of System and Computer Engineering, Carleton University, Ottawa, Ontario, Canada. adler@sce.carleton.ca

be uncorrelated white Gaussian. $\mathbf{J}$ is calculated from the FEM as $\mathbf{J}_{ij} = \left.\frac{\partial \mathbf{y}_i}{\partial \mathbf{x}_j}\right|_{\boldsymbol{\sigma}_1}$. This system is underdetermined since $n_N > n_M$, and regularization techniques are needed to calculate a conductivity change estimate, $\hat{\mathbf{x}}$, which is faithful to both the measurements, $\mathbf{y}$, and to *a priori* constraints on a "reasonable" image.

A. Least Squares (ℓ_2 norm) solution

The LS solution of (1) can be obtained using GN method which seeks a solution $\hat{\mathbf{x}}$ by minimizing

$$\|\mathbf{y} - \mathbf{J}\mathbf{x}\|^2_{\Sigma_n^{-1}} + \|\mathbf{x} - \mathbf{x}_0\|^2_{\Sigma_x^{-1}} \tag{2}$$

where $\|\cdot\|^2$ is the ℓ_2 norm, and the norm subscript is the weight matrix, such that $\|\mathbf{x}\|^2_{\mathbf{W}} = \sum_i \sum_j \mathbf{x}_i \mathbf{W}_{ij} \mathbf{x}_j$. $\mathbf{x}_0$ is the *a priori* mean conductivity change. $\boldsymbol{\Sigma}_n \in \mathbb{R}^{n_M \times n_M}$ is the covariance matrix of the measurement noise $\mathbf{n}$. Since $\mathbf{n}$ is uncorrelated, $\boldsymbol{\Sigma}_n$ is a diagonal matrix with $[\boldsymbol{\Sigma}_n]_{i,i} = \sigma_i^2$, where σ_i^2 is the noise variance at measurement i. $\boldsymbol{\Sigma}_x \in \mathbb{R}^{n_N \times n_N}$ is the expected image covariance. Let $\mathbf{W} = \sigma_n^2 \boldsymbol{\Sigma}_n^{-1}$ and $\mathbf{R} = \sigma_x^2 \boldsymbol{\Sigma}_x^{-1}$. $\mathbf{W}$ and $\mathbf{R}$ are heuristically determined *a priori*. Here σ_n is the average measurement noise amplitude and σ_x is the *a priori* amplitude of conductivity change.

By solving (2) and defining a hyperparameter $\lambda = \sigma_n/\sigma_x$, a linearized, one-step inverse solution is obtained [6]

$$\hat{\mathbf{x}} = \left(\mathbf{J}^T\mathbf{W}\mathbf{J} + \lambda^2\mathbf{R}\right)^{-1} \mathbf{J}^T\mathbf{W}\mathbf{y} = \mathbf{B}\mathbf{y} \tag{3}$$

where $\mathbf{B} = \left(\mathbf{J}^T\mathbf{W}\mathbf{J} + \lambda^2\mathbf{R}\right)^{-1} \mathbf{J}^T\mathbf{W}$ is the linear, one-step inverse. λ controls the trade-off between resolution and noise attenuation in the reconstructed image.

If image elements are assumed to be independent with identical expected magnitude, $\mathbf{R}$ becomes an identity matrix, $\mathbf{I}$, and (3) uses zeroth-order Tikhonov regularization. For EIT, such solutions tend to push reconstructed noise toward the boundary, since the measured data is much more sensitive to boundary image elements. Instead, $\mathbf{R}$ may be scaled with the sensitivity of each element, so that $\mathbf{R}$ is a diagonal matrix with elements $[\mathbf{R}]_{i,i} = \left[\mathbf{J}^T\mathbf{J}\right]^p_{i,i}$. This is the NOSER prior [4] for an exponent p, where $p \in [0, 1]$. The TV prior is the discretization of the gradient operator. the TV of a 2D image is the sum of the variation across each mesh edges, with each edge weighted by its length [7]. In this paper, the TV prior is used to calculate the matrix $\mathbf{R}$.

B. ℓ_1 norm solution

When applied to the image prior $\|\mathbf{x} - \mathbf{x}_0\|$, ℓ_2 norm solutions tend to give "smoothed" images, because the prior applies strong penalties to edges. However, strong edges are physiologically realistic, and are desired in the images. Although edge blur can be decreased using a small hyperparameter, λ, this dramatically decreases noise performance. Another method is to carefully define a prior with *a priori* knowledge of edge locations [8]. However, this approach can result in image artefacts that appear plausible, and thus hard to detect (*e.g.*, [9]), if the prior information is too detailed, but does not describe the actual image.

The Total Variation (TV) of the ℓ_1 norm is known to work well to preserve intrinsic edges in original images. However, ℓ_1 norm solutions are difficult because the objective function is non-differentiable and cannot be efficiently solved with traditional linearization techniques. Minimization of functions of TV norms normally uses iterative methods. The primal dual interior point method (PD-IPM) was proposed [10] to solve the TV minimization problem by removing the singularity points which caused non-differentiability before applying the linearization method. A mixed norm TV solution [7] for EIT was formulated as:

$$\hat{\mathbf{x}} = \underset{\mathbf{x}}{argmin}\, \|\mathbf{y} - \mathbf{J}\mathbf{x}\|^2_2 + \|\mathbf{x} - \mathbf{x}_0\|^1 \tag{4}$$

where $\|\cdot\|^2$ is the ℓ_2 norm and $\|\cdot\|^1$ is the ℓ_1 norm weighted by the TV prior.

Another attractive property of ℓ_1 solution is its resistance to data outliers. For the data residue term, $\mathbf{y} - \mathbf{J}\mathbf{x}$, the ℓ_2 norm is highly sensitive to data outliers, because it assumes a Gaussian distribution, which over weights the significance of large outliers. The ℓ_1 solution is inherently more robust against outliers in measurements because it does not square each measurement misfit. This property of ℓ_1 regularization is promising, especially for EIT, because measurement errors constitute one of primary technical obstacles of clinical EIT, where erroneous electrodes introduce severe artefacts [11].

We propose applying ℓ_1 regularization to both the data residual and the image prior; the optimization problem becomes

$$\hat{\mathbf{x}} = \underset{\mathbf{x}}{argmin}\, \|\mathbf{y} - \mathbf{J}\mathbf{x}\|^1 + \|\mathbf{x} - \mathbf{x}_0\|^1 \tag{5}$$

A well known algorithm to the sum of ℓ_1 norms is Iteratively Reweighted Least Squares (IRLS) [12]. The IRLS method iteratively solves a weighted least squares problem which begins as an ℓ_2 norm, and converges to the ℓ_1 norm solution.

C. Generalized ℓ_1 and ℓ_2 regularization with iterative method

A weighted and regularized inverse may be generally formulated as

$$\hat{\mathbf{x}} = \underset{\mathbf{x}}{argmin}\, \|\mathbf{y} - \mathbf{J}\mathbf{x}\|^{p_n}_{\boldsymbol{\Sigma}_n^{-1}} + \|\mathbf{x} - \mathbf{x}_0\|^{p_x}_{\boldsymbol{\Sigma}_x^{-1}} \tag{6}$$

where p_n and p_x are the data and image norms and must be ≥ 1 for stability. The norm subscript is the weight matrix, such that $\|\mathbf{x}\|^p_{\mathbf{W}} = \sum_i \sum_j \mathbf{x}_i^{p/2} \mathbf{W}_{ij} \mathbf{x}_j^{p/2}$. A weighted p norm With $p_n = p_x = 2$, both term use ℓ_2 norms, equivalent to (2), and denoted ℓ_2-ℓ_2. With $p_n = 2, p_x = 1$ it models the implementation of (4), and is denoted ℓ_2-ℓ_1. In this paper, a general iterative algorithm for (6) is developed, which allows flexible choice of combinations of norms by simply choosing difference p_n and p_x. A similar ℓ_k norm choosing method can be found in [13].

(6) is reformulated in quadratic forms:

$$\begin{aligned}\hat{\mathbf{x}} = \underset{\mathbf{x}}{argmin}&(\mathbf{y} - \mathbf{J}\mathbf{x})^t \mathbf{D}_n^t \boldsymbol{\Sigma}_n^{-1} \mathbf{D}_n (\mathbf{y} - \mathbf{J}\mathbf{x}) + \\ &(\mathbf{x} - \mathbf{x}_0)^t \mathbf{D}_x^t \boldsymbol{\Sigma}_x^{-1} \mathbf{D}_x (\mathbf{x} - \mathbf{x}_0)\end{aligned} \tag{7}$$

where $\mathbf{D}_n$ is a diagonal matrix in which

$$[\mathbf{D}_n]_{i,i} = ([|\mathbf{y} - \mathbf{Jx}|]_i)^{\frac{1}{2}p_n - 1}. \quad (8)$$

here $|\cdot|$ is the absolute value. Similarly, $\mathbf{D}_x$ is a diagonal matrix with

$$[\mathbf{D}_x]_{i,i} = ([|\mathbf{x} - \mathbf{x}_0|]_i)^{\frac{1}{2}p_x - 1} \quad (9)$$

Note that for $p_n = 2$ or $p_x = 2$, $\mathbf{D}_n$ or $\mathbf{D}_x$ will be the identity matrix. When $p_n = 1$ or $p_x = 1$, $[\mathbf{D}_n]_{i,i} = ([|\mathbf{y} - \mathbf{Jx}|]_i)^{-\frac{1}{2}}$ or $[\mathbf{D}_x]_{i,i} = ([|\mathbf{x} - \mathbf{x}_0|]_i)^{-\frac{1}{2}}$. In order to remove singular points where $[|\mathbf{y} - \mathbf{Jx}|]_i$ or $[|\mathbf{x} - \mathbf{x}_0|]_i$ equal zero, (8) and (9) are modified as follows

$$[\mathbf{D}_n]_{i,i} = ([|\mathbf{y} - \mathbf{Jx}|]_i + \beta)^{\frac{1}{2}p_n - 1} \quad (10)$$

$$[\mathbf{D}_x]_{i,i} = ([|\mathbf{x} - \mathbf{x}_0|]_i + \beta)^{\frac{1}{2}p_x - 1} \quad (11)$$

where β is a small positive scalar.

This formulation leads to an iterative update expression for calculation of $\hat{\mathbf{x}}$; the $k+1$ iteration $\hat{\mathbf{x}}^{(k+1)}$ is calculated from $\hat{\mathbf{x}}^{(k)}$ using

$$\hat{\mathbf{x}}^{(k+1)} = \mathbf{x}^{(k)} + \left(\mathbf{J}^t\mathbf{W}(\mathbf{x}^{(k)})\mathbf{J} + \lambda^2\mathbf{R}(\mathbf{x}^{(k)})\right)^{-1} \mathbf{J}^t\mathbf{W}(\mathbf{x}^{(k)})\left(\mathbf{y} - \mathbf{Jx}^{(k)}\right) \quad (12)$$

where

$$\mathbf{W}(\mathbf{x}) = \sigma_n^2\mathbf{D}_n(\mathbf{x})^t\mathbf{\Sigma}_n^{-1}\mathbf{D}_n(\mathbf{x}) \quad (13)$$

$$\mathbf{R}(\mathbf{x}) = \sigma_x^2\mathbf{D}_x(\mathbf{x})^t\mathbf{\Sigma}_x^{-1}\mathbf{D}_x(\mathbf{x}) \quad (14)$$

III. SIMULATIONS

Four EIT reconstruction types were tested on the proposed algorithm: ℓ_2 norms on both the data residue and the image prior parts (ℓ_2-ℓ_2); ℓ_2 norm on the data residue part and ℓ_1 norm on image prior (ℓ_2-ℓ_1); ℓ_1 on the data residue part and ℓ_2 norm on image prior (ℓ_1-ℓ_2); ℓ_1 norm on both parts (ℓ_1-ℓ_1).

Algorithms were implemented for evaluation of 2D EIT problems using the EIDORS software [9]. Numerical simulations were conducted using an FEM model with 576 elements. Illustrated as Fig. 1: 16 electrodes (marked as green dots) were simulated surrounding the medium, using an adjacent stimulation and measurement pattern. Inside this model, there were two inhomogeneous areas with conductivity 2.0, while the background had conductivity 1.0. The noise performance of the algorithms was tested by adding pseudo random, zero mean Gaussian noise with a fixed random seed. $NSR = 1\%$ where NSR is the ratio of noise to signal power. Images were reconstructed on a 1024 element model which differs from the simulation model to avoid the *inverse crime* [14].

The proposed algorithm was tested with ten iterations. The TV prior was used for all algorithms. Hyperparameters were chosen empirically for the best comprise between image resolution and noise performance. If the ℓ_1 norm was applied on data residue, $\lambda = 1.0$, elsewhere, $\lambda = 0.01$.

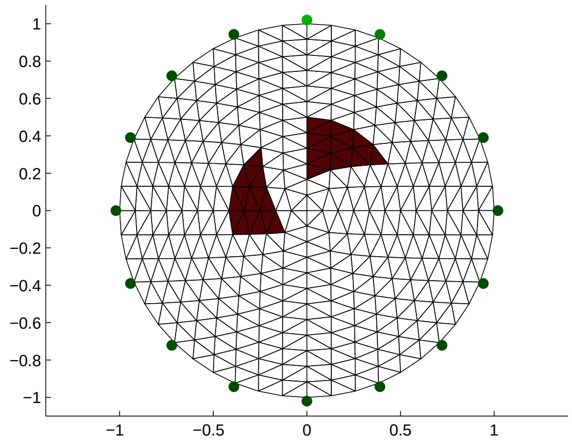

Fig. 1. Simulation finite element model with 576 elements. Electrodes are indicated by green dots. The background and inhomogeneities have conductivities 1.0 and 2.0, respectively.

IV. RESULTS

Images were calculated from simulation data using the algorithms discussed in this paper. Fig. 2, compares the reconstructed images from the various choices of ℓ_1 and ℓ_2 prior. (a) is equivalent to the conventional GN method by choosing the ℓ_2-ℓ_2 norm combination. When applied to the image prior, the ℓ_1 norm obtains better edge sharpness and less artefacts than the ℓ_2 norm.

In order to evaluate the data error robustness of the different norm types, data errors (outliers) were deliberately introduced. Assuming that for certain electrode malfunction, the measurement failure rate was 5% where electrodes cannot sense voltages. The measurement failure happens randomly. In this simulation, this erroneous effect was implemented by randomly choosing 10 (out of 208) data and set them as zeros. By repeating the same reconstructions as Fig. 2, the corresponding "electrode-error" images are generated, and shown in Fig. 3. When ℓ_2 norm is used for the data residue term, the reconstructed image shows only noise (Fig. 3(a)(b)); however, with the ℓ_1 norm on the data residue (Fig. 3(c)(d)) the reconstructed images are very similar to the error free case. This shows high resistance of ℓ_1 solutions against data errors.

V. DISCUSSION

EIT images reconstructed using an ℓ_1 norm formulation give two distinct advantages: edge preservation (when ℓ_1 norm is applied to the image priors term), and error robustness (when applied to the data residue term). However, the disadvantage is that the ℓ_1 norm formulation cannot be computed as a linear one-step reconstruction due to non-differentiability. Thus, ℓ_1 norm image reconstruction requires an iterative algorithm which is computationally efficient. In this paper, an efficient iterative method for EIT reconstruction is proposed, which allows, arbitrary choice of data and

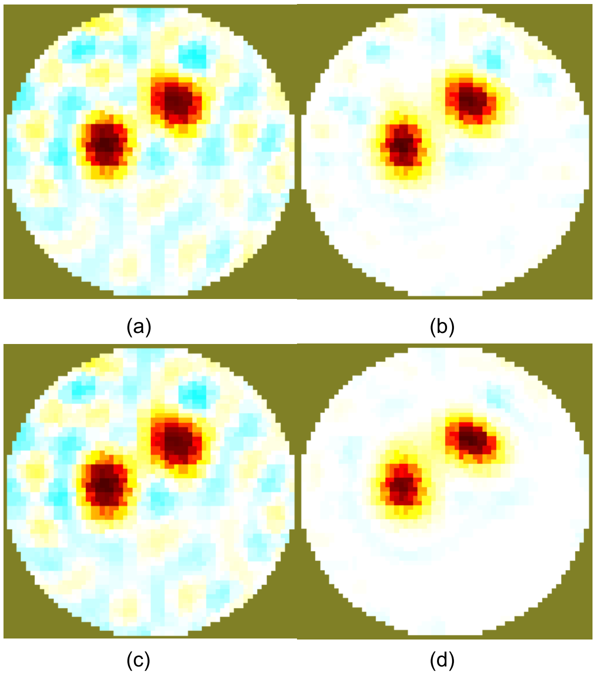

Fig. 2. Images reconstructed using different ℓ_1 and ℓ_2 norms: (a)$p_n = 2, p_x = 2$ (ℓ_2-ℓ_2), (b)$p_n = 2, p_x = 1$ (ℓ_2-ℓ_1), (c)$p_n = 1, p_x = 2$ (ℓ_1-ℓ_2), (d)$p_n = 1, p_x = 1$ (ℓ_1-ℓ_1).

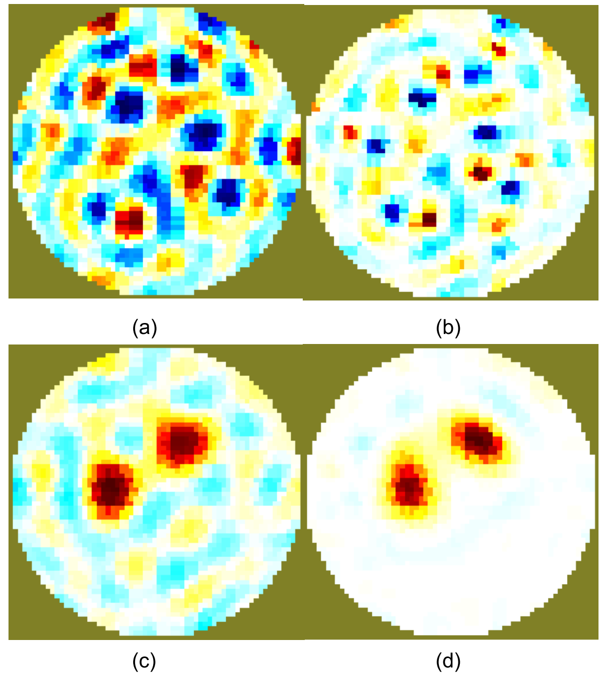

Fig. 3. Electrode error was added to data. Images reconstructed with different data norms: (a)$p_n = 2, p_x = 2$ (ℓ_2-ℓ_2); (b)$p_n = 2, p_x = 1$ (ℓ_2-ℓ_1); (c)$p_n = 1, p_x = 2$ (ℓ_1-ℓ_2); (d)$p_n = 1, p_x = 1$ (ℓ_1-ℓ_1)

image prior norms (p_n and p_x) to be implemented. Results suggest that ℓ_1 norms on both terms provide the best images in terms of image resolution and robustness to data noise.

REFERENCES

[1] W. Lionheart, N. Polydorides, and A. Borsic, *Electrical impedance tomography: methods, history and applications*. Bristol and Philadelphia: IOP, 2005, ch. 1: The Reconstruction Problem.

[2] M. Vauhkonen, P. Karjalainen, and J. Kaipio, "A Kalman filter approach to track fast impedance changes in electrical impedance tomography," *IEEE Trans. Biomed. Eng.*, vol. 45, pp. 486–493, 1998a.

[3] N. Polydorides and W. Lionheart, "A Matlab toolkit for three-dimensional electrical impedance tomography: A contribution to the Electrical Impedance and Diffuse Optical Reconstruction Software project," *Meas. Sci. Technol.*, vol. 13, pp. 1871–1883, 2002.

[4] M. Cheney, D. Isaacson, J. Newell, S. Simske, and J. Goble, "NOSER: an algorithm for solving the inverse conductivity problem," *Int.J.Imaging Syst.Technol.*, vol. 2, pp. 66–75, 1990.

[5] B. Graham and A. Adler, "Electrode placement configurations for 3d EIT," *Physiol.Meas.*, vol. 28, pp. S29–S44, 2007.

[6] A. Adler, T. Dai, and W. Lionheart, "Temporal image reconstruction in electrical impedance tomography," *Physiol. Meas.*, vol. 28, pp. S1–S11, 2007.

[7] A. Borsic, B. Graham, A. Adler, and W. Lionheart, "Total variation regularization in electrical impedance tomography," *submitted*, 2007.

[8] J. Kaipio, V. Kolehmainen, M. Vauhkonen, and E. Somersalo, "Construction of nonstandard smoothness priors," *Inverse Problems*, vol. 15, pp. 713–729, 1999.

[9] A. Adler and W. Lionheart, "Uses and abuses of EIDORS: An extensible software base for EIT," *Physiol. Meas.*, vol. 27, pp. S25–S42, 2006.

[10] T. Chan, G. Golub, and P. Mulet, "A nonlinear primal-dual method for total variation-based image restoration," *SIAM Journal on Scientific Computing*, vol. 20, no. 6, pp. 1964–1977, 1999.

[11] Y. Asfaw and A. Adler, "Automatic detection of detached and erroneous electrodes in electrical impedance tomography," *Physiol. Meas.*, vol. 26, pp. S175–S183, 2005.

[12] J. Scales, A. Gersztenkorn, and S. Treitel, "Fast lp solution of large, sparse, linear systems: Application to seismic travel time tomogrphy," *Journal of Computational Physics*, vol. 75, no. 2, pp. 314–333, 1988.

[13] M. Cetin and W. Karl, "Feature-enhanced synthetic aperture radar image formation based on nonquadratic regularization," *IEEE Trans. Image Processing*, vol. 10, no. 4, pp. 623–631, 2001.

[14] R. K. D. Colton, *Inverse Acoustic and Electromagnetic Scattering Theory*. Berlin: Springer, 1998.